ACS APPLIED MATERIALS & INTERFACES

Research Article

www.acsami.org

Hierarchical Microstructures Formed by Bidisperse Colloidal Suspensions within Colloid-in-Liquid Crystal Gels

Heberth Diestra-Cruz,[†] Emre Bukusoglu,[‡] Nicholas L. Abbott,*[,‡] and Aldo Acevedo*[,†]

[†]Department of Chemical Engineering, University of Puerto Rico-Mayagüez, Mayagüez 00681, Puerto Rico

[‡]Department of Chemical and Biological Engineering, University of Wisconsin-Madison, Madison, Wisconsin 53706, United States

Supporting Information

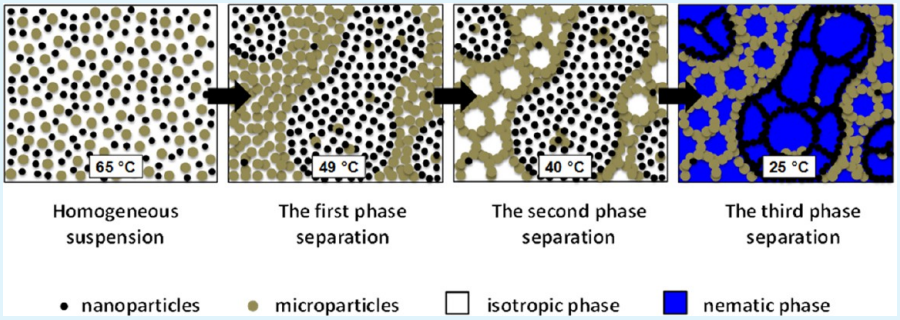

ABSTRACT: Past studies have reported that colloids of a single size dispersed in the isotropic phase of a mesogenic solvent can form colloid-rich networks (and gels) upon thermal quenching of the system across the isotropic−nematic phase boundary of the mesogens. Herein we report the observation and characterization of complex hierarchical microstructures that form when bidisperse colloidal suspensions of nanoparticles (NPs; iron oxide with diameters of 188 ± 20 nm or poly(methyl methacrylate) with diameters of 150 ± 15 nm) and microparticles (MPs; polystyrene with diameters of 2.77 ± 0.20 μm) are dispersed in the isotropic phase of 4-pentyl-4′-cyanobiphenyl (5CB) and thermally quenched. Specifically, we document microstructuring that results from three sequential phase separation processes that occur at distinct temperatures during stepwise cooling of the ternary mixture from its miscibility region. The first phase transition demixes the system into coexisting MP-rich and NP-rich phases; the second promotes formation of a particle network within the MP-rich phase; and the third, which coincides with the isotropic-to-nematic phase transition of 5CB, produces a second colloidal network within the NP-rich phase. We quantified the dynamics of each demixing process by using optical microscopy and Fourier transform image analysis to establish that the phase transitions occur through (i) surface-directed spinodal decomposition, (ii) spinodal decomposition, and (iii) nucleation and growth, respectively. Significantly, the observed series of phase transitions leads to a hierarchical organization of cellular microstructures not observed in colloid-in-liquid crystal gels formed from monodisperse colloids. The results of this study suggest new routes to the synthesis of colloidal materials with hierarchical microstructures that combine large surface areas and organized porosity with potential applications in catalysis, separations, chemical sensing, or tissue engineering.

KEYWORDS: *colloid-in-liquid crystal gels, bidisperse suspensions, microparticles, nanoparticles, spinodal decomposition, hierarchical microstructure, rheology*

1. INTRODUCTION

Nematic liquid crystals (LCs) are fluids within which the molecular constituents exhibit long-range orientational order.[1] This orientational order is easily altered by external perturbations, such as shear stresses or applied electric and magnetic fields, thus making LCs the basis of a widely explored class of stimuli-responsive materials.[1] Recent studies have also shown that LCs can be used to direct suspensions of colloidal particles to organize into percolating networks, leading in some cases to the formation of so-called colloid-in-liquid crystal gels (CLCGs).[2−5] These materials, which comprise cellular domains of LCs separated by colloid-rich networks, exhibit the rheological characteristics of solid-like gels yet can also retain the responsiveness of the LCs. This promising class of composite materials has been explored as the basis of chemical and biological sensors,[6,7] smart glasses,[4,8] and responsive substrates for cell culture.[9]

The majority of past studies of CLCGs has started with monodisperse colloids dispersed in an isotropic phase of mesogens. Network formation was observed when the dispersion was cooled through the isotropic-to-nematic phase boundary.[2] At the isotropic-to-nematic transition temperature (T_{NI}), nematic domains were observed to nucleate and grow, expelling colloids into the remaining isotropic regions to

Received: December 21, 2014
Accepted: February 23, 2015
Published: February 23, 2015

DOI: 10.1021/am509008m
ACS Appl. Mater. Interfaces 2015, 7, 7153−7162

minimize elastic strain of the LC phase induced by the colloids.[10] The resulting cellular colloidal network transforms the viscoelastic properties of the material into that of a solid-like gel at room temperature.[11−13] The above-described LC-templated synthesis of colloidal networks has been observed for a wide variety of colloids, including poly(methyl methacrylate) (PMMA),[12] gold,[14] polymerized divinylbenzene,[15] CdSe/ZnS quantum dots,[16] and composite magnetic microspheres.[17]

Recently, an alternative pathway leading to the synthesis of CLCGs was reported by Bukusoglu et al.[5] In contrast to prior studies, when using polystyrene microparticles (MPs), phase separation of the MPs (into a network) was observed to occur within the isotropic phase of the mesogens (i.e., prior to cooling to the isotropic-to-nematic phase boundary). During the initial stage of this phase separation process, the characteristic sizes (L) of the domains were observed to be invariant with increasing time, consistent with the predictions of Cahn−Hilliard theory for the linear regime of spinodal decomposition (SD).[18] In addition, the domains were observed to coarsen with a power law behavior, $L \sim t^n$, with n approaching 1/3 for thick samples, as predicted for the diffusive regime of SD.[19] Although subsequent cooling across T_{NI} did not produce significant changes in microstructure, it did compact the MPs within the network, as evidenced by changes in rheology (a solid-like gel was formed).

Whereas the above-described past studies of CLCGs have employed colloids of a single size, it is well-known from the studies of the phase behavior of colloidal dispersions in isotropic solvents that a bimodal size distribution can lead to a rich variety of phases not observed in monodisperse systems.[20−23] Motivated by these past studies of bidisperse colloidal systems in isotropic solvents, herein we report an investigation of the influence of bimodal particle size distributions on the microstructures of CLCGs. We hypothesized that the use of mixtures of colloids with different sizes might lead to microstructures not found in monodisperse CLCGs and thus provide the basis of methods for the synthesis of new classes of colloidal materials.

As detailed in this paper, we present the first evidence that hierarchical microstructures do form when using bimodal particle suspensions of NPs and MPs in 5CB. Significantly, the hierarchical microstructures were observed to arise via three sequential phase separation processes during the stepwise cooling of colloidal suspensions from the miscibility region of the ternary mixture. By quantifying the time-dependent evolution of the microstructures, the mechanism underlying each phase separation process was determined. We found, for example, that wetting of the confining surfaces played a central role in the first phase separation, and its influence on the system morphology is presented in detail. By elucidating these processes, we identify key parameters that can be used to tune the hierarchical architectures of the CLCGs formed by bidisperse colloidal dispersions. As noted earlier, colloidal materials that possess a hierarchy of structural length scales are highly desirable for applications in catalysis,[24] separations,[25] chemical sensing, or tissue engineering[26] since, for example, transport properties defined by organized porosity can be combined with the high surface areas associated with the fine structural features (e.g., for adsorption or reactions).[27] Although the focus of this paper is on characterization and elucidation of fundamental processes that lead to the formation of the hierarchical microstructure (it is not focused on demonstrations of functional properties), we do show the generality of this approach as the basis of a synthetic methodology by using both inorganic (iron oxide) and polymeric (PMMA) NPs. In future studies, we plan to introduce functional nanoparticles (e.g., nanoparticles for catalysis) into these materials and explore these materials in the context of catalysis and adsorptive separation processes.

2. EXPERIMENTAL SECTION

2.1. Materials. The mesogen 4-pentyl-4′-cyanobiphenyl (5CB) was purchased from Sigma-Aldrich (St. Louis, MO) and used without further purification. T_{NI} of 5CB was determined to be 35.0 °C by differential scanning calorimetry (TA Instruments Q2000). Magnetic polystyrene microspheres (MMPs) with an average diameter of 2.7 μm (Cat. No. PM-20-10) and nonmagnetic MPs with an average diameter of 2.3 μm (Cat. No. PP-20-10) were purchased from Spherotech (Lake Forest, IL). Of particular relevance to this study, the MMPs were prepared by the manufacturer with a layer of iron oxide NPs coating a polystyrene core.[28] As detailed in the Supporting Information (SI), we found that incubation of the MMPs in the isotropic phase of 5CB led to the release of the iron oxide NPs from the MMPs. The iron oxide NPs released from the MMPs were measured to form clusters with an average diameter (by dynamic light scattering) of 188 ± 20 nm, a size that was consistent with TEM images of the NPs (see Figure S1, SI). The remaining MPs (of polystyrene) were determined to have diameters of 2.77 ± 0.20 μm. By thermogravimetric analysis (TA Instruments TA-2950), the NP content of MMPs was found to be 12.3 wt %. The binary mixtures of MPs and NPs used in the experiments reported in this paper were prepared by release of the NPs from MMPs. Poly(methyl methacrylate) (PMMA) particles with a diameter of 150 ± 15 nm (Cat. No. PM150NM) were purchased from Magsphere Inc. (Pasadena, CA). All particles were received as aqueous suspensions.

2.2. Sample Preparation. In brief, MMPs were washed three times in DI water and recovered by centrifugation for 5 min at 9000 rpm.[5,17] At each step, following removal of the supernatant, the colloids were resuspended in DI water using sonication. The colloids were then dried in a vacuum oven at 50 °C for at least 1 week. The MMPs were mixed with 5CB in an Eppendorf tube and then heated to 65 °C (above the T_{NI} of 5CB) in a water bath and vortexed and sonicated for at least 6 h to obtain a binary mixture of MPs and iron oxide NPs (see above and the SI for details).

2.3. Optical Characterization. To study the evolution of the morphology of the ternary mixture, an Olympus BX51 polarized optical microscope equipped with an INSTEC HSC302-mK1000A temperature controller and a digital camera was used. The glass slides were cleaned of organic surface contaminants by using a PE-200 Plasma Etching Benchtop System. Optical cells were fabricated by gluing with an epoxy resin that set in 5 min and two cleaned glass slides that were separated by Mylar spacers of the desired thicknesses. Next, the optical cells were preheated at 65 °C and filled with the ternary mixture (MPs, NPs, and 5CB) by capillary action. To remove any concentration gradients within the sample and to prevent convective flows, the filled optical cells were equilibrated above 65 °C overnight. In addition to the above-described optical cells, rectangular glass capillaries (Cat. No. 5002; VitroCom, Mountain Lakes, NJ) were used to evaluate the effects of surfaces on the phase separation process (details below). To rapidly quench the sample from 65 °C, the filled cells or glass capillaries were quickly transferred from a hot plate at ∼65 °C to a thermal stage positioned on a microscope, which was pre-equilibriated at a desired temperature T (<65 °C).

2.4. Image Analysis. Bright-field optical micrographs were used to study the time evolution of the characteristic sizes of the microstructures that formed upon cooling the samples. The evolution of the morphology was recorded as a function of time, and then images at fixed time intervals were extracted using software that converted video to JPG (DVD Videosoft). ImageJ software was used to calculate the radial average of the 2D Fast Fourier Transforms (FFT) and thus obtain the structure factor, $S(Q,t)$, as a function of the wavenumber, Q, and time, t, for each optical image. The structure factors were fit to

DOI: 10.1021/am509008m
ACS Appl. Mater. Interfaces 2015, 7, 7153−7162

Gaussian functions using the Igor Pro 6.32A software. The wavenumber associated with the position of the peak of the structure factor, Q_m, was obtained from the Gaussian fit. The characteristic length of the phase-separated system (L) was calculated as $2\pi/Q_m$.

2.5. Rheology. We measured the temperature-dependent dynamic mechanical properties of the three-component system (5CB, NPs, MPs) using a rheometer (Physica MCR-302; Anton Paar) with parallel plates (25 mm diameter) and a gap of 0.3 mm. Unless otherwise stated, dynamic measurements were performed in an oscillatory mode at a frequency of 1 Hz, strain amplitude of 0.5%, and constant cooling rate of 1 °C/min. The frequency and strain values were confirmed to correspond to the linear viscoelastic regime of the material. Before cooling the samples and measuring the temperature-dependent properties, samples were presheared at 80 °C to ensure that the initial state of the system corresponded to a homogeneous dispersion of the colloids.

3. RESULTS AND DISCUSSION

3.1. Overall Description of the Microstructuring. As described in the Experimental Section, we observed the MPs and NPs (of iron oxide) to form homogeneous suspensions in the isotropic phase of 5CB at 65 °C. Figure 1 summarizes the most important stages of the sequential phase separation processes that were initiated by the cooling of dispersions (films with thickness of 20 μm) that contained 11.6 wt % of MPs and 1.6 wt % of NPs. The uniform distribution of NPs is evidenced in Figure 1a by the homogeneous brown hue across the sample (Figure 1a). Due to near matching of the refractive indices of the MPs and isotropic 5CB, the MPs are not seen at 65 °C. As the temperature of the sample was cooled at a rate of 1 °C/min from the miscibility region, the onset of phase separation was observed at 50 °C. This temperature is defined as T_{PS}. To characterize the isothermal evolution of this phase separation process, the system was imaged at 49 °C (1 °C below T_{PS}, and called T_1) following a fast quench from 65 °C. At 49 °C, the system was observed to demix into NP-rich (identified by the brown color of magnetic colloids) and NP-poor regions. Figure 1b shows the early stages (20 s) of the demixing process during which a highly interconnected bicontinuous morphology was observed. At longer times, the morphology of the system transitioned to a dispersion of discrete NP-rich disk-like regions (darker regions in Figure 1c). The size of the disk-like regions increased with time and ultimately reached a lateral size on the order of 100 μm, which is several times greater than the thickness of the sample (20 μm). As will be shown below, the NP-poor regions evident in Figure 1c are rich in MPs.

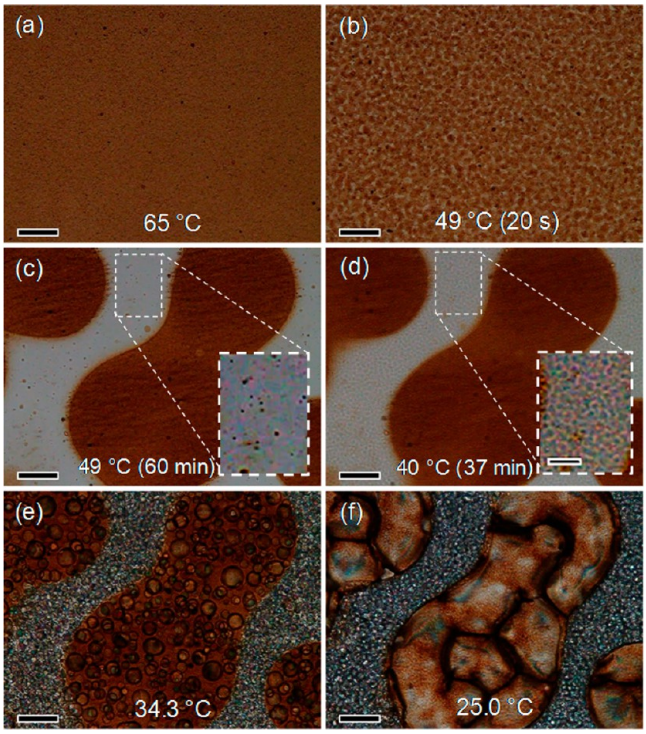

Figure 1. Microstructures formed by sequential phase transitions within a mixture of 11.6 wt % MPs, 1.6 wt % NPs, and 5CB. Bright-field micrographs of (a) the initial homogeneous suspension in the isotropic phase of 5CB (scale bars: 50 μm), (b,c) the system after a first phase transition (dark regions are NP-rich, light regions are MP-rich phases), (d) the system after a second phase transition, and (e,f) the system after a third phase transition. Insets in (c) and (d) show magnified regions in the sample with scale bars corresponding to 20 μm. The image contrast in the magnified images was enhanced to permit observation of the microstructure.

Further cooling of the sample below 49 °C resulted in the initiation of a second phase separation process (Figure 1d). Specifically, following a fast quench from 49 to 40 °C (i.e., a temperature between T_{PS} and T_{NI} of the 5CB), we observed the MPs to segregate from 5CB to form a MP network within the NP-poor regions of the sample. The formation of this MP network confirmed the presence of the MPs in these domains. The inset in Figure 1d shows the morphology of the network formed by the MPs after equilibration for 37 min at 40 °C. Redistribution of colloids within the NP-rich phase was not visible during the phase separation process occurring at 40 °C (Figure 1d) due to the strong absorbance of the NPs. However, observations described in the SI when using PMMA NPs do provide evidence of reorganization of the MPs in the NP-rich phase during this second phase separation (see below for details).

Finally, upon cooling from 40 to 34.5 °C, the T_{NI} of the 5CB in the mixture (which is ~0.5 °C lower than T_{NI} of pure 5CB),[3,11] we observed a third demixing process. As shown in Figure 1e, this third phase separation process was characterized by the nucleation of nematic droplets throughout the system. In the NP-rich regions, the nematic domains expelled NPs toward the boundaries of these regions (Figure 1f). In contrast, only minor changes on the overall shapes of the MP-rich domains were observed during the third phase separation; i.e., the sizes and shapes of these domains were highly determined by the second phase separation process. Overall, this third phase transition yielded a hierarchically microstructured material with distinctly different LC domain sizes in the MP-rich and NP-rich regions of the sample (Figure 1f). To summarize our observations, both the thermal time course (Figure 2a) and a schematic representation of MP and NP distributions at the end of each phase separation process (Figure 2b) are shown in Figure 2. Additional support for the cartoons shown in Figure 2b is presented in the remainder of this paper.

3.2. Quantitative Characterization of the Dynamics of Microstructure Formation. *First Phase Transition: Surface-Directed Spinodal Decomposition.* Figure 3 details the time-dependent evolution of the system morphology during the first phase separation process at 49 °C. As noted above, at short times (t < 40 s), the segregation of NPs into a bicontinuous morphology composed of NP-rich (MP-poor) and MP-rich phases was observed (Figure 3a). The microstructure coarsened (see characteristic length, L, in Figure 3c) while maintaining the

DOI: 10.1021/am509008m
ACS Appl. Mater. Interfaces 2015, 7, 7153−7162

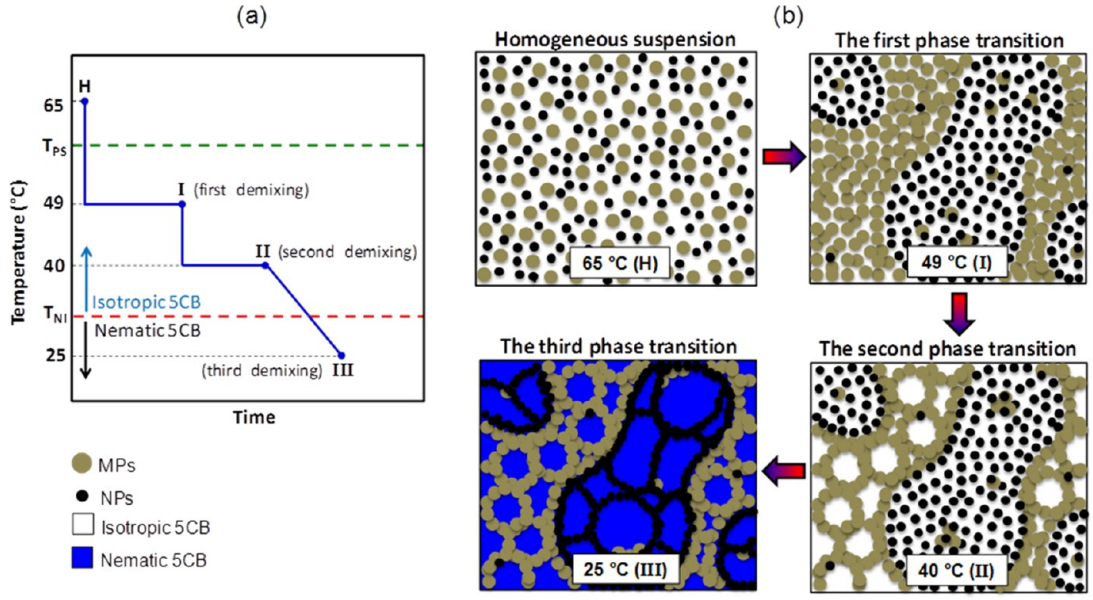

Figure 2. (a) Schematic representation of the thermal history of the samples characterized in this study and (b) a cartoon showing the temperature-dependent formation of hierarchical microstructure that results from use of bidisperse colloidal mixtures.

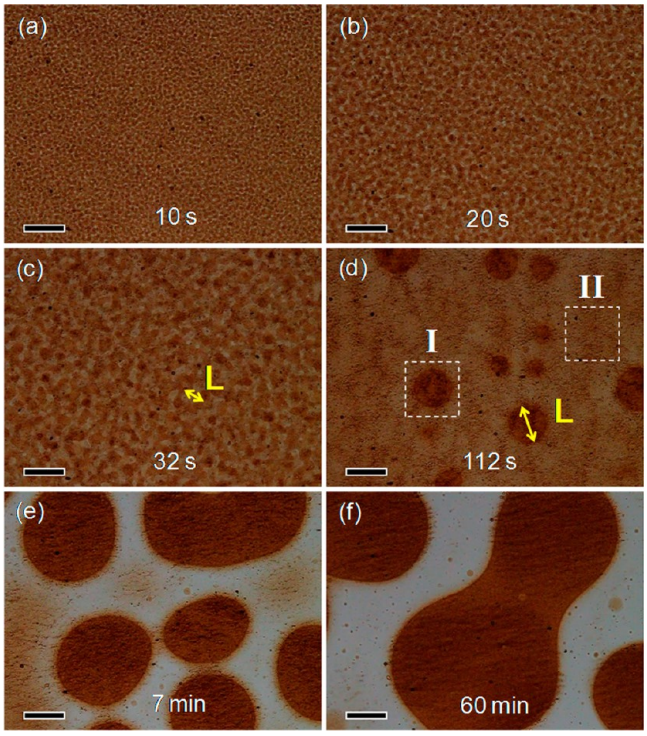

Figure 3. Bright-field micrographs of a mixture of 11.6 wt % MPs, 1.6 wt % NPs, and 5CB undergoing a phase transition that was triggered by thermal quenching from 65 to 49 °C. (a) 10 s, (b) 20 s, (c) 32s, (d) 112 s, (e) 7 min, and (f) 60 min. Scale bars: 50 μm.

bicontinuous morphology (Figures 3b and c), consistent with self-similar growth.[29] We note here that self-similar growth of bicontinuous morphologies has been observed previously in systems undergoing phase separation via SD.[30] In our experiments, when L approached the sample thickness ($L \sim h$), a transition in morphology to a discrete domain structure was observed (Figure 3d). Domains with high concentrations of NPs were observed in some regions (see square I in Figure 3d), whereas regions of low but uniform concentration of NPs were observed in other regions of the sample (see square II in Figure 3d). During this second stage of growth (t > 40 s), each of the NP-rich domains did not grow at the same rate, and a distribution of domain sizes was observed (Figure 3d). In addition, the lateral size of some NP-rich regions (L in Figure 3d) increased with time (Figure 3d–f), while other NP-rich domains vanished.

Although the initial stage of the phase separation is consistent with the typical bicontinuous morphology associated with a process of SD, to provide further insight into the mechanism of phase separation, the time-dependent change in L was quantified from optical micrographs by Fourier transform analysis (see Experimental Section for details). As shown in Figure 4a, during the initial growth stage (<40 s) at 49 °C, a characteristic structural peak, typical of systems with periodic patterns, was observed. This peak shifted toward smaller wavenumbers indicating growth of the average size of the domains with increasing time. Inspection of Figure 4b reveals that we do not observe a period of growth of the microstructure at constant L ($L \sim 1/Q_m$), as is predicted by theories of SD and has been experimentally observed.[18] The absence of this regime has also been noted in past studies and in some cases has been attributed to fast kinetics arising from low viscosity.[31] As coarsening of the microstructure progressed, L was determined to follow a power law behavior, $L \sim t^n$, where the growth exponent, n, reaches a value of 3/2 at ~30 s (Figure 4b). This nonlinear behavior ending with a large growth exponent (i.e., 3/2) has been previously reported in binary fluid mixtures undergoing surface-directed spinodal decomposition (SDSD).[32] Specifically, the large exponent of 3/2 is attributed to selective wetting of one phase on the walls confining the system.[33] On the basis of dimensional analysis, Tanaka[34] proposed that the fast growth exponent (i.e., 3/2) is a consequence of the pressure-induced hydrodynamic transport of the wetting phase from the bicontinuous region in the bulk to wetting layers at the confining walls and obtained the relation $L \sim [(\sigma/\eta)t]^{3/2}$, where σ is the surface tension and η is the viscosity (see Figure 4c for schematic illustration). This physical view has been shown to be consistent with other

DOI: 10.1021/am509008m
ACS Appl. Mater. Interfaces 2015, 7, 7153–7162

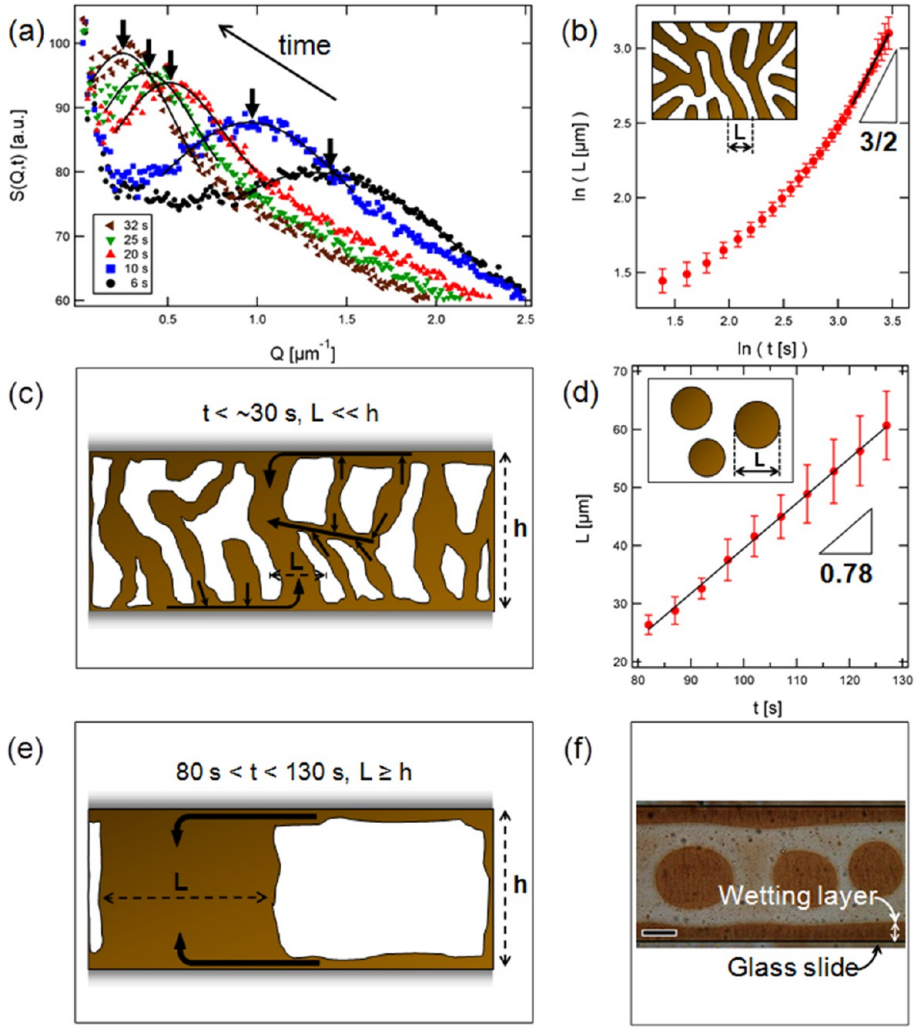

Figure 4. Time evolution of the microstructure of a mixture of 11.6 wt % MPs, 1.6 wt % NPs, and 5CB (following the onset of a phase transition initiated by quenching to 49 °C). (a) Structure factor as a function of wavenumber and time. (b) Change in L during the initial stage of the phase transition (t < 40 s). The inset shows a schematic illustration of the bicontinuous morphology. (c) Schematic representation of the process occurring in (b). (d) Average size (L) of disk-like NP-rich regions as a function of time during the final stage of the phase transition. (e) Schematic representation of the final stage of the phase transition. (f) Bright-field optical micrograph showing the wetting layer on the walls of a rectangular glass capillary 20 min after the onset of the phase transition. Scale bar: 50 μm.

experimental observations[33] and numerical simulations.[35] It is also consistent with our observations regarding the small NP-rich domains ($L \ll h$). A flow of the NP-rich phase toward the wetting layer causes small domains to disappear, thus generating regions of the sample that are largely free of NP-rich domains (square II in Figure 3d).

When $L \geq h$, the NP-rich domains bridge the two confining surfaces (square I in Figure 3d), and a new regime of domain growth is observed. In the framework of the above-described model, for the period of time over which the thickness of the wetting layer does not substantially change, a linear relationship, $L \sim t$, has been predicted, corresponding to a flow of material from the wetting layers to growing domains.[34] To test this prediction against our experimental measurements, the time dependence of the average lateral size of NP-rich disk-like domains (L in Figure 3d) was measured during the second stage of the dynamic process (t > 40 s). These measurements were obtained by characterizing domains with initial size $L \approx$ 25 μm for a subsequent period of time during which coalescence of domains was not observed (80 s < t < 130 s). During this time period, a scaling of $L \sim 0.78t$ was observed (Figure 4d,e), consistent with the above-proposed mechanism.

To provide additional evidence for the formation of wetting layers on the glass surfaces that confine the ternary mixture (and which we interpret to influence the coarsening dynamics), we performed an experiment using a rectangular glass capillary with a thickness of 20 μm and a width of 200 μm. Figure 4f shows the system morphology 20 min after the onset of the phase separation at 49 °C. Wetting layers of the NP-rich phase (darker regions) are observed at the glass walls perpendicular to the viewing plane (lateral walls), while NP-rich disk-like domains were observed far away from the lateral walls. Also, according to the SDSD mechanism, the number of NP-rich disk-like domains is expected to increase with decrease in cell thickness since it is easier to obtain domains with $L \sim h$.[36] This qualitative behavior was observed in our ternary system. Overall, our results support the proposal that the first phase transition in the ternary mixture occurred via SDSD. However, a question remains, namely, the origin of the driving force for the segregation of MPs and NPs during this phase transition. We address this question below.

DOI: 10.1021/am509008m
ACS Appl. Mater. Interfaces 2015, 7, 7153−7162

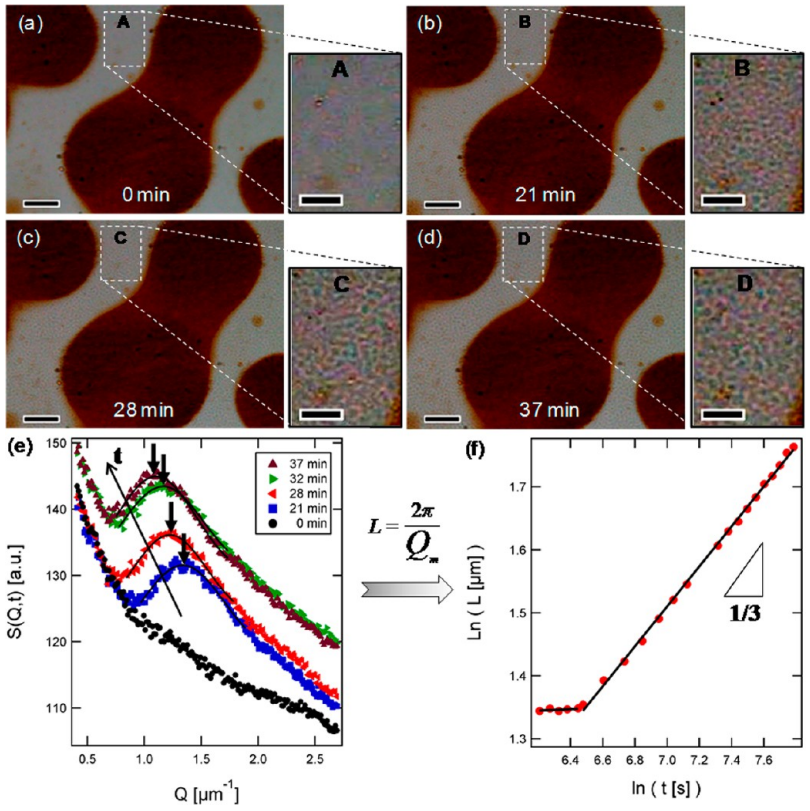

Figure 5. Time evolution of the microstructure of a mixture of 11.6 wt % MPs, 1.6 wt % NPs, and 5CB following a phase transition induced by a rapid quench from 49 to 40 °C. (a–d) Bright-field micrographs collected at the indicated times following the onset of phase separation. Scale bars: 50 μm. Dashed rectangles show magnified regions on the figure. Scale bars (inset): 20 μm. The contrast in the micrographs was enhanced to permit observation of the microstructure in these images. (e) Structure factor as a function of the wavenumber and time. (f) Variation of L as a function of time.

Recently, Bukusoglu et al.[5] showed that MPs (1 μm in diameter) and a mixture of mesogens called E7 can phase separate within the isotropic phase of E7 via SD (upon thermal quenching). On the basis of this past study, we hypothesized that the demixing of MPs and 5CB drives the phase transition of our ternary system. To test this hypothesis, we performed experiments in a binary system composed of 2.3 μm MPs and 5CB. We determined the phase separation temperature (T_{PS}) for a 12 wt % MP/5CB system to be 48.5 °C, which is similar to (1.5 °C below) the T_{PS} of the ternary mixture containing the MPs and NPs. This small difference in the T_{PS} suggests that the presence of the NPs only modifies to a small extent (increases) the interparticle interaction between MPs driving the phase separation (shifts the phase boundary to slightly higher temperatures). This result is consistent with past studies that have shown that addition of nonadsorbing polymers or nanoparticles to a suspension of micrometer-sized particles can induce an effective attraction between the large colloids via a so-called depletion interaction.[37] Furthermore, after quenching the binary system described above (MPs + 5CB) from 65 °C (miscibility region) to 47.5 °C (1 °C below T_{PS}), we observed the binary system to exhibit the same morphology as the ternary system (Figure S2, SI). Overall, this result leads us to conclude that the demixing of the 5CB and MPs largely drives the initial phase separation of our ternary system and that the NPs partition away from the resulting MP-rich phase. We also note that the system morphology that arises from this first phase transition can be tuned by changing the demixing time, cell thickness, or temperature quench depth (Figure S3, SI).

Time Evolution of the Second Phase Transition: Spinodal Decomposition. At the end of the first phase transition (initiated by the decrease in temperature to T_1), the system comprised disk-like NP-rich domains (with lateral sizes >100 μm) dispersed in a continuous MP-rich phase. At temperatures below T_1 and above T_{NI} of 5CB (35 °C), we observed a second phase transition to take place. Figure 5 shows the time evolution of the second demixing process at 40 °C (after a fast quench from T_1 = 49 °C). This phase separation occurred primarily within MP-rich regions and involved the segregation of MPs from the isotropic 5CB to form a cellular network over time (Figure 5a–d). We note that the initial morphology of the system (cellular microstructure) at short times (following the onset of the second phase transition) was similar to that detailed previously by Bukusoglu et al.[5] (corresponding to SD). Figure 5a–d also shows that the NPs remained well-dispersed within the NP-rich domains at 40 °C. Specifically, we did not observe substantial changes in the morphology of the NP-rich domains during the phase transition evident in the MP-rich domains at 40 °C.

We also quantified the dynamics of the second phase separation process. Here we note that while the quench to approximately 40 °C occurred within 1 min it took seven additional minutes to fully stabilize the temperature (see Figure S4, SI). Although the domain size L is influenced by changes in temperature during the stabilization period, we found that the dynamics of the phase separation process, which are related to

DOI: 10.1021/am509008m
ACS Appl. Mater. Interfaces 2015, 7, 7153–7162

the variation of L and not with the absolute magnitude of L, are not affected significantly by the short-time dynamics (see below). For this reason, we only analyzed the structure factors 8 min after the onset of the temperature quench. The structure factors are shown in Figure 5e (see Figure S5, SI). With the elapse of time, a characteristic peak in the structure factor (domain size) shifts toward smaller wavenumbers, indicating that the domain size in the system increases over time. Inspection of Figure 5f reveals that $L \sim t^{1/3}$, consistent with the diffusive regime of spinodal decomposition.[19] As noted above, the morphology and dynamics of this phase separation are similar to that reported by Bukusoglu et al. for an analogous system that was rapidly quenched and underwent spinodal decomposition.[5] This similarity in dynamics and morphology leads us to conclude that the second phase separation within the MP-rich regions of the ternary mixture proceeds via SD. The scaling predictions associated with SD can thus be used to describe the effects of particle concentration, time of phase separation, and quench depth on the microstructure that emerge during this phase separation, as detailed previously.[5]

Evolution of the Third Phase Transition Process: Nucleation and Growth. Figure 6 shows the evolution of the system microstructure caused by the third phase transition, which was initiated by cooling at a rate of 0.5 °C/min from 40 °C (see Figure 2 for details of the thermal profile) through T_{NI} (~34.5 °C). The first sign of the third phase transition was the nucleation of nematic domains in both MP-rich and NP-rich regions (Figure 6a,b). In the NP-rich regions, the nematic domains expel NPs into the isotropic 5CB, consistent with the effects of particle-induced elastic strain of the LC.[10,38,39] This process leads to the formation of an interconnected NP network within the NP-rich regions (Figure 6c). In addition, as shown in Figures 6c and d, an additional consequence of this phase transition is the formation of a thin layer of NPs at the interface between MP-rich and NP-rich regions. This nucleation and growth mechanism is similar to that reported in earlier studies of monodisperse colloids in LCs.[12,14,17] In contrast, in the MP-rich regions of the composite material, the phase transition of the 5CB does not cause significant changes to the MP network (Figure 6d). This arises because the nucleation and growth of the nematic phase occurs within the 5CB-rich domains formed during the second phase transition at 40 °C. This observation is consistent with the dynamics observed for the MP/E7 binary system.[5] As can be seen in Figure 6d, at the end of the third phase transition, a composite material with a hierarchical microstructure is obtained at room temperature.

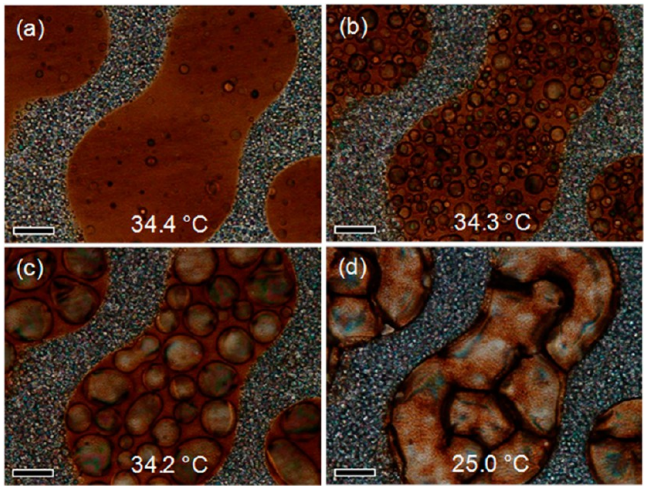

Figure 6. Bright-field micrographs of the microstructure of a ternary mixture of 11.6 wt % MPs, 1.6 wt % NPs, and 5CB following the third phase transition during cooling at 0.5 °C/min. (a) 34.4 °C, (b) 34.3 °C, (c) 34.2 °C, and (d) 25.0 °C. Scale bars: 50 μm.

Generality of the Sequence of Phase Transitions. We also performed an experiment to explore the generality of the above-described LC-templated process that yields a hierarchically microstructured composite material. The experiment involved replacement of the iron oxide NPs with PMMA NPs of similar size (150 nm in diameter). Past studies have reported that PMMA demixes from 5CB via a mechanism involving nucleation and growth at T_{NI} of 5CB.[11] For a suspension containing 10 wt % of MPs and 2 wt % of PMMA, we measured a first phase separation process to begin at 52 °C (T_{PS}), which is similar to (2 °C above) the T_{PS} of the ternary mixture with the iron oxide NPs. Additional characterization of the PMMA/MP/5CB system yielded phase transitions and microstructures similar to those reported for the iron oxide NP/MP/5CB mixture (Figure S6, SI). Note that inspection of Figure S6 (SI) reveals reorganization of the MPs in the PMMA NP-rich phase during the second phase separation process. Overall, we conclude that the formation of the hierarchical microstructured composite is not limited to just iron oxide NPs but appears to be a potentially broadly applicable way of microstructuring colloidal materials.

Phase Diagram. The microstructures described above are interpreted to arise from processes triggered by the passage of the system across thermodynamic phase boundaries (by cooling), and thus we summarize our observations with reference to a qualitative phase diagram of this system. As depicted in Figure 7, the ternary system is considered as a pseudobinary mixture with one phase composed of 5CB and NPs and the other phase comprised of 5CB and MPs (as discussed in Section 3.1). At 65 °C (point H), the NPs and MPs are homogeneously dispersed in the isotropic phase of 5CB (miscibility region). The system is then quenched from 65 °C to T_I, which moves the system inside the spinodal region of

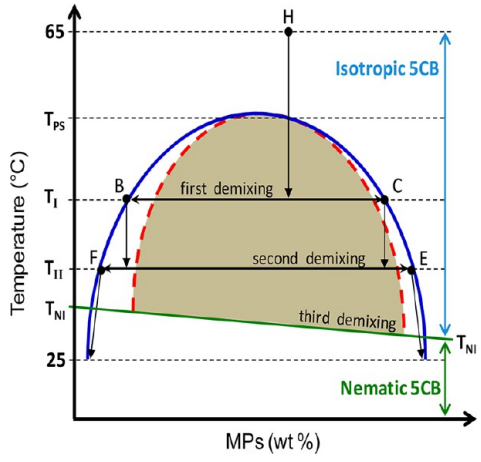

Figure 7. Schematic representation of the thermodynamic pathway leading to the hierarchical microstructure reported in this paper. The ternary mixture is represented as a pseudobinary phase diagram. Dotted (red) and solid (blue) lines correspond to the spinodal and binodal curves, respectively.

DOI: 10.1021/am509008m
ACS Appl. Mater. Interfaces 2015, 7, 7153−7162

the phase diagram. At T_I, the first phase separation proceeds via SDSD and separates the system into points B and C on the phase diagram, corresponding to NP-rich and MP-rich phases, respectively. Subsequent rapid quenching from T_I to T_{II} leads to the initiation of demixing processes between MPs and the 5CB within each of the subphases formed during the first phase separation. We note that the rate of quenching from T_I to T_{II} is sufficiently fast that the NP- and MP-rich domains behave effectively as independent systems. The MP-rich phase (point C) falls into the unstable region and separates again via SD. This second phase separation induces the formation of the MP network (point E) within the MP-rich domains created in the first phase separation process. The MPs within the NP-rich domains also reorganize upon quenching to T_{II}, and there is presumably some small (not measurable) evolution in the MP composition of the NP-rich phase, as shown in Figure 7. Finally, when the system is quenched from T_{II} to 25 °C (room temperature), a third phase separation takes place at the T_{NI} of the 5CB. The phase transition of 5CB within the NP-rich phase reorganizes the NPs, while the morphology of MP-rich regions remains largely unaltered.

3.3. Confirmation of Gelation. Past studies have shown that CLCGs formed from monodisperse colloids can exhibit solid-like properties.[2−5] To characterize the effects of the hierarchical microstructure observed in the bidisperse composites on the dynamic mechanical properties, we performed temperature ramp and frequency sweep measurements using a rheometer. Figure 8a shows the temperature dependence of the storage (G') and loss (G'') modulus of a 13.2 wt % mixture of MPs and NPs in 5CB upon cooling from 65 to 25 °C at 1 °C/min. We note here that optical micrographs confirmed that at this cooling rate the ternary mixture forms a microstructure that is very similar to that detailed above (see Figure S7, SI). At 65 °C, inspection of Figure 8a reveals that G' is lower than G'', consistent with the anticipated signature of a liquid-like material. Upon cooling, G'' exhibited a peak between 50 and 47 °C, with the onset of the peak coinciding with the onset of the first phase separation process identified previously by optical microscopy (Section 3.1). In addition, the width of the peak coincides with the temperature range over which the bicontinuous microstructure formed and then evolved during the first phase separation (50−49 °C). Specifically, the decrease in the modulus upon cooling below 49 °C coincides with the transition from the bicontinuous network to the NP-rich disk-like domains (see Section 3.2). Thus, this particular rheological signature correlates with two distinct stages of the first phase transition.

Upon cooling below 47 °C, G'' increased from ∼3 Pa at 47 °C to ∼20 Pa at 34 °C, while G' reached ∼10 Pa at 34 °C. Because the system was cooled continuously at a rate of 1 °C/min, the second phase separation processes (formation of the MP network; see Section 3.2) occurred almost immediately after the first phase separation, i.e., after the formation of the MP-rich continuous phase. The formation of the MP-rich network thus appears to be responsible for the continuous increase in modulus upon cooling to T_{NI}. This conclusion is consistent with results reported previously for a system comprised of MPs and E7.[5] During this interval of temperatures, $G' < G''$, indicating that the system continued to exhibit liquid-like behavior.

Upon passing through the T_{NI} of 5CB (∼34.5 °C), both G' and G'' exhibited a sudden increase in magnitude, reaching G' ∼ 2500 Pa and G'' ∼ 3000 Pa at 25 °C. The abrupt increase

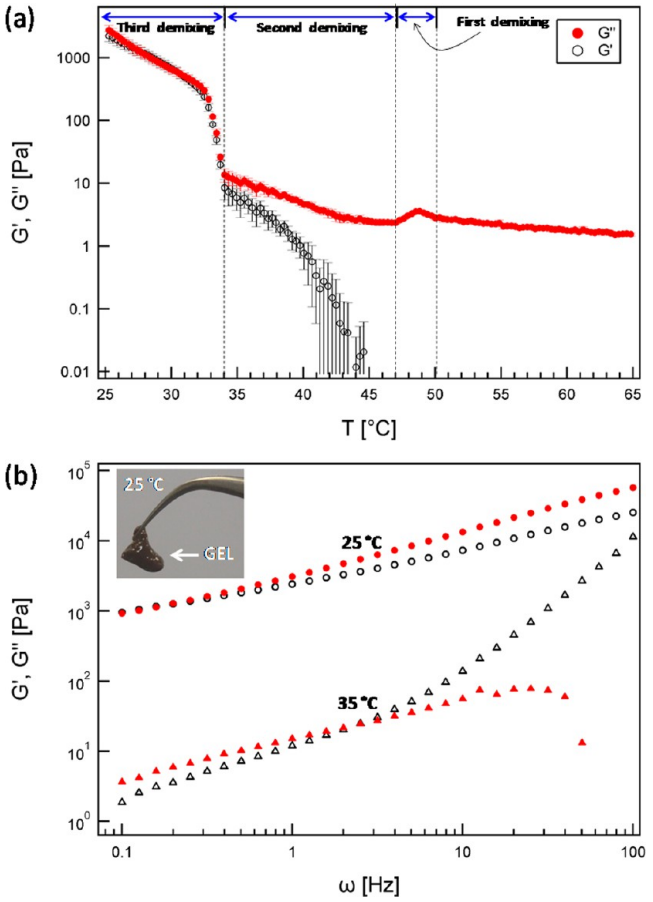

Figure 8. (a) Temperature and (b) frequency dependence of storage (G', open symbols) and loss (G'', filled symbols) moduli of a ternary mixture of 11.6 wt % MPs, 1.6 wt % NPs, and 5CB during continuous cooling at 1 °C/min.

likely arises from two contributions, namely, the compaction of the MPs within the network in the MP-rich phase (as detailed in ref 5) and the formation of the second NP network within the NP-rich regions (Figure 6d). As discussed above, both processes are induced by the phase transition of the 5CB (see Section 3.2).

Finally, Figure 8b shows G' and G'' as a function of frequency at temperatures above (35 °C) and below (25 °C) the T_{NI} of 5CB. For the measurement at 35 °C, we observed a crossover from liquid-like ($G' < G''$) to solid-like ($G' > G''$) behavior with increasing frequency to occur at ∼2.5 Hz, whereas at 25 °C a crossover from solid-like to liquid-like behavior with increasing frequency occurred at ∼0.2 Hz. Overall, these results are similar to those of a past study of the MP/E7 system (at 37 °C, within the nematic phase of E7, a crossover was found at 0.1 Hz).[5] The reader is referred to this prior study for a detailed discussion of these rheological signatures.

We note that the elastic modulus rises strongly at 35 °C for frequencies above 3 Hz. This behavior has been reported previously in past studies of aqueous suspensions of polystyrene particles, but the origins of it are not yet fully understood.[40] However, consistent with the observation of solid-like mechanical properties at 25 °C, as illustrated in the inset of Figure 8b, we show that the hierarchical composite formed from MPs and NPs is a self-standing gel.

DOI: 10.1021/am509008m
ACS Appl. Mater. Interfaces 2015, 7, 7153−7162

4. CONCLUSIONS

This study reports a complex LC-templated pathway that leads to the formation of hierarchical colloidal microstructures via three sequential phase transitions involving bidisperse colloidal suspensions in a mesogenic solvent. Significantly, the origins of the hierarchical structure of the composite can be traced to a first phase transition that proceeds by SDSD, a second phase transition that occurs via SD, and a third phase transition induced by the isotropic-to-nematic phase transition of the 5CB. This understanding provides a rational basis for the design and optimization of the hierarchical microstructure. The hierarchical organization of colloids observed in our study suggests the basis of a versatile synthetic methodology that will permit the preparation of colloidal materials with organized pores and high surface areas. In future studies, we will explore the incorporation of functional NPs into these composites and their application in catalysis and adsorptive separations.

■ ASSOCIATED CONTENT

Supporting Information

Measurements characterizing colloid sizes, additional micrographs of the phase separation processes, and details regarding the temperature profiles. This material is available free of charge via the Internet at http://pubs.acs.org.

■ AUTHOR INFORMATION

Corresponding Authors

*E-mail: abbott@engr.wisc.edu. Phone: +1 (608) 265 5278.
*E-mail: aldo.acevedo@upr.edu. Phone: +1 (787) 832 4040. Ext. 2473.

Notes

The authors declare no competing financial interest.

■ ACKNOWLEDGMENTS

This study was funded primarily by the National Science Foundation through the Wisconsin - Puerto Rico Partnership for Research and Education in Materials (DMR-0934115) and the Materials Research Science and Engineering Center (DMR-1121288), with additional partial support from the Army Research Office (W911NF-14-1-0140 and W911NF-11-1-0251)

■ REFERENCES

(1) de Gennes, P. G.; Prost, J. *The Physics of Liquid Crystals*, 2nd ed.; Oxford University Press: Oxford, 1995.
(2) Meeker, S. P.; Poon, W. C. K.; Crain, J.; Terentjev, E. M. Colloid-Liquid Crystal Composites: an Unusual Soft Solid. *Phys. Rev. E* **2000**, *61*, R6083−R6086.
(3) Petrov, P. G.; Terentjev, E. M. Formation of Cellular Solid in Liquid Crystal Colloids. *Langmuir* **2001**, *17*, 2942−2949.
(4) Wood, T. A.; Lintuvuori, J. S.; Schofield, A. B.; Marenduzzo, D.; Poon, W. C. K. A Self-Quenched Defect Glass in a Colloid-Nematic Liquid Crystal Composite. *Science* **2011**, *7*, 79−83.
(5) Bukusoglu, E.; Pal, S. K.; de Pablo, J. J.; Abbott, N. L. Colloid-in-Liquid Crystal Gels Formed via Spinodal Decomposition. *Soft Matter* **2014**, *10*, 1602−1610.
(6) Pal, S. K.; Agarwal, A.; Abbott, N. L. Chemically Responsive Gels Prepared from Microspheres Dispersed in Liquid Crystals. *Small* **2009**, *5*, 2589−2596.
(7) Agarwal, A.; Sidiq, S.; Setia, S.; Bukusoglu, E.; de Pablo, J. J.; Pal, S. K.; Abbott, N. L. Colloid-in-Liquid Crystal Gels that Respond to Biomolecular Interactions. *Small* **2013**, *9*, 2785−2792.
(8) van Boxtel, M. C. W.; Janssen, R. H. C.; Bastiaansen, C. W. M.; Broer, D. J. Viscoelastic Liquid Crystal Colloids for the Continuous Processing of Twisted Nematic Electro-Optical Cells. *J. Appl. Phys.* **2001**, *89*, 838−842.
(9) Agarwal, A.; Huang, E.; Palecek, S.; Abbott, N. L. Optically Responsive and Mechanically Tunable Colloid-in-Liquid Crystal Gels that Support Growth of Fibroblasts. *Adv. Mater.* **2008**, *20*, 4804−4809.
(10) Ullrich, B.; Auernhammer, G. K.; Sam, E. M.; Vollmer, D. Tracer Colloids Close to an Isotropic-Nematic Domain Interface with Phase Transition-Induced Solute Transport. *Colloids Surf., A* **2010**, *354*, 298−307.
(11) Anderson, V. J.; Terentjev, E. M.; Meeker, S. P.; Crain, J.; Poon, W. C. K. Cellular Solid Behavior of Liquid Crystal Colloids 1. Phase Separation and Morphology. *Eur. Phys. J. E* **2001**, *4*, 11−20.
(12) Roth, M.; D'Acunzi, M.; Vollmer, D.; Auernhammer, G. K. Viscoelastic Rheology of Colloid-Liquid Crystal Composites. *J. Chem. Phys.* **2010**, *132*, 124702.
(13) Anderson, V. J.; Terentjev, E. M. Cellular Solid Behavior of Liquid Crystal Colloids 2. Mechanical Properties. *Eur. Phys. J. E* **2001**, *4*, 21−28.
(14) Milette, J.; Cowling, S. J.; Toader, V.; Lavigne, C.; Saez, I. M.; Lennox, R. B.; Goodby, J. W.; Reven, L. Reversible Long Range Network Formation in Gold Nanoparticle-Nematic Liquid Crystal Composites. *Soft Matter* **2011**, *8*, 173−179.
(15) Yamamoto, T.; Yoshida, M. Viscoelastic and Photoresponsive Properties of Microparticle/Liquid-Crystal Composite Gels: Tunable Mechanical Strength along with Rapid-Recovery Nature and Photochemical Surface Healing using an Azobenzene Dopant. *Langmuir* **2012**, *28*, 8463−8469.
(16) Rodarte, A. L.; Pandolfi, R. J.; Ghosh, S.; Hirst, L. S. Quantum Dot/Liquid Crystal Composite Materials: Self-Assembly Driven by Liquid Crystal Phase Transition Templating. *J. Mater. Chem. C* **2013**, *1*, 5527−5532.
(17) Diestra-Cruz, H.; Rinaldi, C.; Acevedo, A. Rheological, Optical and Thermal Characterization of Temperature-Induced Transitions in Liquid Crystal Ferrosuspensions. *J. Appl. Phys.* **2012**, *111*, 07B308.
(18) Cahn, J. W. Phase Separation by Spinodal Decomposition in Isotropic Systems. *J. Chem. Phys.* **1965**, *42*, 93−99.
(19) Siggia, E. D. Late Stages of Spinodal Decomposition in Binary Mixtures. *Phys. Rev. A* **1979**, *20*, 595−605.
(20) Sikorski, M.; Sandy, A. R.; Narayanan, S. Depletion-Induced Structure and Dynamics in Bimodal Colloidal Suspensions. *Phys. Rev. Lett.* **2011**, *106*, 188301.
(21) Xu, W.; Nikolov, A. D.; Wasan, D. T. Role of Depletion and Surface-Induced Structural Forces in Bidisperse Suspensions. *AIChE J.* **1997**, *43*, 3215−3222.
(22) Dinsmore, A. D.; Yodh, A. G.; Pine, D. J. Phase Diagrams of Nearly-Hard-Sphere Binary Colloids. *Phys. Rev. E* **1995**, *52*, 4045−4057.
(23) Zhou, J.; van Duijneveldt, J. S.; Vincent, B. Two-Stage Phase Separation in Ternary Colloid−Polymer Mixtures. *Phys. Chem. Chem. Phys.* **2011**, *13*, 110−113.
(24) Parlett, C. M. A.; Wilson, K.; Lee, A. F. Hierarchical Porous Materials: Catalytic Applications. *Chem. Soc. Rev.* **2013**, *42*, 3876−3893.
(25) Nakanishi, H.; Norisuye, T.; Tran-Cong-Miyata, Q. Formation of Hierarchically Structured Polymer Films via Multiple Phase Separation Mediated by Intermittent Irradiation. *J. Phys. Chem. Lett.* **2013**, *4*, 3978−3982.
(26) Nam, Y. S.; Park, T. G. Porous Biodegradable Polymeric Scaffolds Prepared by Thermally Induced Phase Separation. *J. Biomed. Mater. Res.* **1999**, *47*, 8−17.
(27) Yao, H. B.; Fang, H. Y.; Wang, X. H.; Yu, S. H. Hierarchical Assembly of Micro-/Nano-Building Blocks: Bio-Inspired Rigid Structural Functional Materials. *Chem. Soc. Rev.* **2011**, *40*, 3764−3785.
(28) Spherotech SPHERO Magnetic Particles. http://www.spherotech.com/para_par.htm (accessed December 15, 2014).
(29) Hashimoto, T.; Itakura, M.; Shimidzu, N. Late Stage Spinodal Decomposition of a Binary Polymer Mixture. II. Scaling Analyses on Qm(τ) and Im(τ). *J. Chem. Phys.* **1986**, *85*, 6773−6786.

DOI: 10.1021/am509008m
ACS Appl. Mater. Interfaces 2015, 7, 7153−7162

(30) Guenoun, P.; Gastaud, R.; Perrot, F.; Beysens, D. Spinodal Decomposition Patterns in an Isodensity Critical Binary Fluid: Direct-Visualization and Light-Scattering Analyses. *Phys. Rev. A* **1987**, *36*, 4876−4890.
(31) Aarts, D. G. a. L.; Dullens, R. P. A.; Lekkerkerker, H. N. W. Interfacial Dynamics in Demixing Systems with Ultralow Interfacial Tension. *New J. Phys.* **2005**, *7*, 40.
(32) Cumming, A.; Wiltzius, P.; Bates, F. S.; Rosedale, J. H. Light-Scattering Experiments on Phase-Separation Dynamics in Binary Fluid Mixtures. *Phys. Rev. A* **1992**, *45*, 885−897.
(33) Shi, B. Q.; Harrison, C.; Cumming, A. Fast-Mode Kinetics in Surface-Mediated Phase-Separating Fluids. *Phys. Rev. Lett.* **1993**, *70*, 206−209.
(34) Tanaka, H.; Araki, T. Wetting Dynamics in a Confined Symmetric Binary Mixture Undergoing Phase Separation. *Phys. Rev. Lett.* **1993**, *70*, 2770−2773.
(35) Tanaka, H. Surface Effects on Spinodal Decomposition of Incompressible Binary Fluid Mixtures. *Europhys. Lett.* **2000**, *51*, 154−160.
(36) Tanaka, H. Interplay Between Wetting and Phase Separation in Binary Fluid Mixtures: Roles of Hydrodynamics. *J. Phys.: Condens. Matter* **2001**, *13*, 4637−4674.
(37) Anderson, V. J.; Lekkerkerker, H. N. W. Insights into Phase Transition Kinetics from Colloid Science. *Nature* **2002**, *416*, 811−815.
(38) Loudet, J. C. Colloidal Inclusions in Liquid Crystals: Phase Separation Mechanisms and some Dynamical Aspects. *Liq. Cryst. Today* **2005**, *14*, 1−14.
(39) West, J. L.; Glushchenko, A.; Liao, G.; Reznikov, Y.; Andrienko, D.; Allen, M. P. Drag on Particles in a Nematic Suspension by a Moving Nematic-Isotropic Interface. *Phys. Rev. E* **2002**, *66*, 012702.
(40) Goodwin, J. W.; Gregory, T.; Miles, J. A.; Warren, B. C. H. The Rheological Properties and the Microstructure of Concentrated Latices. *J. Colloid Interface Sci.* **1984**, *97*, 488−495.

DOI: 10.1021/am509008m
ACS Appl. Mater. Interfaces 2015, 7, 7153−7162